Molecular Cooperative Assembly

DOI: 10.1002/ange.201304034

Three-Dimensional Macroscopic Assemblies of Low-Dimensional Carbon Nitrides for Enhanced Hydrogen Evolution**

*Young-Si Jun, Jihee Park, Sun Uk Lee, Arne Thomas, Won Hi Hong, and Galen D. Stucky**

Nanomaterials feature unique surface, optical, and electronic properties that are often superior to their bulk counterparts. These properties are often interpreted as surface effect and dimensional confinement, which forms the basis to design the nanoscale building blocks or devices for catalysis, electronics, or optics.[1] As these properties are primarily determined by crystallinity, shape, and size of the material, great research efforts have been devoted to the synthesis of nanostructures with well-defined composition and morphology.[2] To date, metals, metal oxides, metal chalcogenides, and organic materials based on molecules and macromolecules have been reported in the form of various nanostructures, ranging from zero-dimensional (0D) nanoparticles, through one-dimensional (1D) nanowires and nanotubes to two-dimensional (2D) nanosheets.[3]

Constructing macroscopic higher-order assemblies out of low-dimensional building blocks as analogues to biological systems is a promising but challenging task.[4] In general, the construction pathway involves 1) the formation of separate nanomaterials and 2) their subsequent integration induced by additional cross-linking agents or structure-directing templates.[5] Mild conditions are essential for creating organic materials owing to their comparable low thermal and mechanical stability. Among the various preparation methods of organic nanostructures, cooperative assembly is a versatile method that enables controlled organization of organic molecules into larger aggregates. Initially formed, well-defined nanostructures can be further organized into higher-order assemblies as amorphous or crystalline close-packed solids by non-covalent interactions, such as hydrogen bonding, π–π stacking, and van der Waals forces.[6] Tailored organic molecules provide a facile route to optimize the materials and develop new structures with complex hierarchy exhibiting properties that are intrinsically different from those of the bulk material or isolated nanomaterials.[7]

Carbon nitrides are, in the ideal case, binary carbon–nitrogen compounds forming a variety of structures from molecular compounds to solid state C/N phases.[8] For example, graphitic carbon nitride (g-C_3N_4) consists of 2D N-bridged tri-*s*-triazine moieties stacked in a graphitic fashion. Polymeric precursors of this ideal g-C_3N_4 have found interest as a metal-free photocatalyst. Polymeric carbon nitride (g-CN) show a bandgap of about 2.7 eV with optoelectronic properties that are sensitively affected by the degree of polymerization.[9] As a polymer, various organic and inorganic processing methods have been applied to modify the texture and photoelectric properties of this material.[10] There are, however, only a few examples of the assembly of even low-dimensional g-CNs into designed nanostructures, as they are difficult to prepare because of the high temperatures needed for their formation. To date, possible pathways are limited to exotemplating (0D and 1D) and thermal exfoliation (2D) strategies.[11] To the best of our knowledge, further integration of g-CN nanostructures into macroscopic higher-order assemblies has yet to be achieved.

Herein, we present a simple method to prepare 3D macroscopic assemblies of low-dimensional g-CNs, such as nanoparticles, nanotubes, and nanosheets. Very recently, supramolecular chemistry of triazine molecules enabled the synthesis of g-CN in the form of hollow spheres.[12] The 2D hexagonal assembly between melamine and cyanuric acid (CA) evolved into nanosheet-like structures during thermal polycondensation without losing its macroscopic morphology. CA or other triazines such as trithiocyanuric acid (TCA) are known to form hydrogen-bonded networks that give rise to preferential crystal structures depending on the donor–acceptor pair and crystallization solvent.[13] Thus it can be expected that "crystal engineering" would allow facile tailoring of textural properties, polycondensation procedures, and interlayer interactions of g-CN. With this in mind we synthesized different hydrogen bonded networks using 1) various donor-acceptor pairs, for example, melamine-cyanuric acid, and -trithiocyanuric acid; 2) different solvents such as dimethyl sulfoxide (DMSO) or H_2O; and 3) different temperatures at which the networks are assembled.

Co-crystals of melamine and cyanuric acid (MCA) were spontaneously formed by mixing equimolar solutions in DMSO at 30 °C (MCA-DMSO-30). The isolated crystals have a hexagonal plate-like morphology with a thickness of

[*] Dr. Y.-S. Jun, Dr. J. Park, Prof. G. D. Stucky
Department of Chemistry and Biochemistry, University of California
Santa Barbara, CA 93106 (USA)
E-mail: stucky@chem.ucsb.edu
Prof. A. Thomas
Department of Chemistry/Functional Materials
Technische Universität Berlin
Hardenbergstrasse 40, 10623 Berlin (Germany)
S. U. Lee, Prof. W. H. Hong
Department of Chemical and Biomolecular Engineering
Korea Advanced Institute of Science and Technology (KAIST)
373-1, Guseong-dong, Yuseong-gu, Daejeon, 305-701 (Korea)

[**] This work was supported by the University of California Lab Fees Research Program and the Project "Light2Hydrogen" of the BMBF (03IS2071D). The MRL Shared Experimental Facilities are supported by the MRSEC Program of the NSF under Award No. DMR 1121053; a member of the NSF-funded Materials Research Facilities Network (www.mrfn.org). We thank Dr. Guang Wu for assistance with single-crystal analysis.

Supporting information for this article is available on the WWW under http://dx.doi.org/10.1002/anie.201304034.

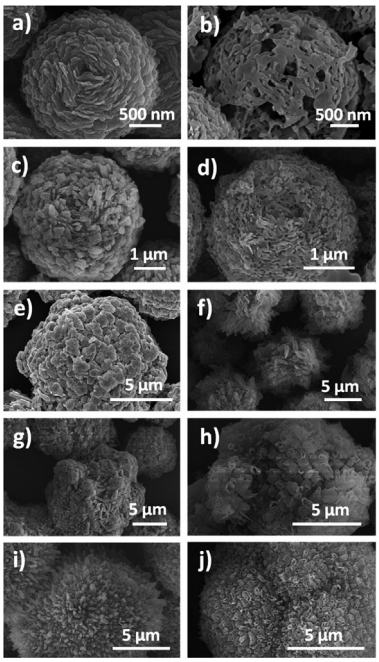

Figure 1. SEM images of as-synthesized MCA-DMSO (left) and the corresponding MCA-DMSO-550 (right) precipitated at a),b) 30, c),d) 60, e),f) 90, g),h) 120, and i),j) 150 °C.

about 40 nm, reflecting the molecular structure, and they are aggregated into 2–3 μm spherical particles (Figure 1 a). The interaction between the plates is easily breakable by post-heating the precipitates in DMSO at above 90 °C for 30 min (Supporting Information, Figure S1). The enhanced solvation at elevated temperatures also reduces hydrogen bonding strength, affecting the number of hydrogen bonds in the hexameric networks and thus the morphology of MCA-DMSO crystals.

To further investigate the temperature effect on the directional formation of the networks, MCA-DMSO was precipitated at temperatures between 60–150 °C (Figure 1 c–i). The transition from hexagonal nanoplates to hexagonal nanorods in the crystal morphology was indeed observed with increasing precipitation temperature. Furthermore, the size of the aggregates was gradually increased from 2 to 10 μm owing to the enhanced solubility. Close-packed arrays of hexagonal nanorods with a thickness of 200 nm were observed in the spherical particles of MCA-DMSO-150 (Supporting Information, Figure S2). The complete aggregation of the remaining hexagonal nanorods into spherical particles requires prolonged precipitation for 30 min at 150 °C (Figure 1 i; Supporting Information, Figure S3). This also induces further growth of hexagonal nanorods and the formation of sea urchin-like structures with solid cores. X-ray diffraction (XRD) patterns and FTIR spectra reveal the same molecular packing and hydrogen bonding interactions of crystal structure for all as-synthesized MCA-DMSO samples (Supporting Information, Figure S4, S5).

MCA-DMSO becomes tri-*s*-triazine-based g-CN by heating at 550 °C under nitrogen.[12] FTIR spectra of MCA-DMSO-550 samples show the peaks centered at 1800–1100 and 800 cm^{-1}, proving the presence of CN heterocyclic ring structures[14] (Supporting Information, Figure S6). XRD patterns of MCA-DMSO-550 samples feature two distinctive peaks indicative of 2D N-bridged tri-*s*-triazine polymer stacked in a graphitic fashion (Supporting Information, Figure S7). The (002) diffraction peak of MCA-DMSO-550 samples at around 27.7° becomes broader and weaker and shifts to slightly lower scattering angles with increasing precipitation temperature. This can be explained by the formation of CN nanotubes with thin wall thickness along with volumetric shrinkage parallel to the direction of the graphitic stacking. In particular, the wall of the nanotube becomes thinner along the lateral direction, that is, the smaller 2D sheet g-CN, and corrugated along the longitudinal direction, namely, the less-perfect interlayer packing motif. This is further evidenced by SEM analysis (Figure 1 b–j).

Hexagonal plates of MCA-DMSO-30 develop the sheet-like structures. Nanoparticles and nanotubes are formed from the rectangular (MCA-DMSO-60) and hexagonal rod-like (MCA-DMSO-90–150) crystals, respectively. It is notable that polycondensation of the aggregates generates the hollow structures without collapsing the 3D organization. Saturated triazine solutions in DMSO lead to the sudden formation of large crystals with defects. A higher defect density at the center of crystals probably induces a higher local sublimation rate of triazine molecules, which would form the hollow structures during polycondensation.[15] A further volume shrinkage in the crystals results from the accompanied mass loss during polycondensation (for example, removal of NH_3) and formation of more condensed structures (Supporting Information, Figure S8).[16] The textural properties of MCA-DMSO-550 samples are summarized in the Supporting Information, Table S1.

So far, it has been shown that temperature control is a convenient way to yield spherical assemblies of g-CN 1D and 2D nanostructures. However, DMSO (MP = 19 °C) as a solvent only allows for a narrow window for temperature control at lower temperature ranges and thus limits the formation of samples with large hexagonal surfaces. CA (or TCA) is known to form 2D sheet structures of its own (especially in water) or in combination with the solvent molecules, which also correlates with the molecular structures of their co-crystals with other monomers in the same solvents.[13,17] This prompted us to examine the crystal structures of MCA and MTCA in the aprotic DMSO and the protic solvent H_2O.

Precipitation of MCA in H_2O at 30 °C (MCA-H_2O-30) only yields bundles of thin microfibers with poor crystallinity which lose the preformed morphology during polycondensation (Supporting Information, Figure S9). To investigate the competitive effect of H_2O on the crystal structure, we precipitate MCA (3.96 mmol) from a good solvent DMSO (420 mmol) in the presence of the poor solvent H_2O. MCA-DMSO-30 indeed undergoes a morphology change at H_2O concentration higher than 7.92 mmol and is mostly transformed into hexagonal nanorods with a thickness of 200 nm and a length of 1 μm at H_2O concentrations higher than 420 mmol. This indicates that the water molecules guide the growth of MCA precipitates in the longitudinal direction by competing for the hydrogen bonding. We therefore employed

hydrothermal conditions to increase the solubility of MCA in H_2O. A MCA-H_2O-30 dispersion was first prepared as a precursor and then transferred into an autoclave for hydrothermal treatment at 180 °C for 4 h. The thin microfibers of MCA-H_2O-30 were indeed completely transformed into hexagonal microfibers with a thickness of 1 μm and a length of up to 10 μm (Figure 2 a). The XRD pattern of MCA-H_2O-180 coincides well with that of the single crystal-

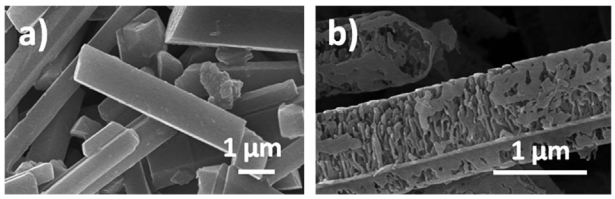

Figure 2. SEM images of a) MCA-H_2O-180 and b) the corresponding MCA-H_2O-180-550.

line material bearing the in-plane 2D hexagonal pattern and graphitic stacking (JCPDS no. 00-005-0127; Supporting Information, Figure S10). Both MCA-DMSO and MCA-H_2O have the same crystal structure, for which the directional preference on the growth significantly depends on the crystallization solvent. Figure 2 b shows a SEM image of MCA-H_2O-180 heated to 550 °C for 4 h. The preformed morphology was well-maintained during the polycondensation without volumetric shrinkage. A certain degree of hydrogen bonding (or more precisely the large 2D sheet formation) rather than π–π interactions is crucial to avoid the structure collapse because 1) the covalent connection via trigon nitrogen formed between melem or melon motifs endows the g-CNs with high thermal stability up to 600 °C and 2) the covalent connection is only formed between the molecular motifs placed on the same 2D sheets. Interestingly, inside the hexagonal hollow microfibers there remained layered sheet-like structures about 15 nm in thickness supported by the outer surface of the hollow microfiber to maintain the vertical alignment.

The effect of the precursor monomers on the directional formation of triazine networks was investigated by using TCA instead of CA as co-monomer. Precipitation from the equimolar solutions induces the formation of rectangular microfibers with large 2D sheet area irrespective of the crystallization solvent (Supporting Information, Figure S11). MTCA-DMSO/H_2O-30 and MTCA-H_2O-100 crystals have a length of 6–8 μm and a width of about 1 μm, which further extends to a length of 60 μm and a width of 10 μm in MTCA-DMSO-30. High-resolution SEM images reveal the layered packing of the desired 2D sheet-like structures in MTCA crystals. Packing analysis using the single-crystalline MTCA-DMSO-30 shows that melamine and TCA are held together by multiple hydrogen bonds, π–π interactions, and also electrostatic interactions (see the section on single-crystal analysis in the Supporting Information for details).

The desired 2D sheet-like structures of g-CN with a large graphene area were successfully obtained by heating MTCA crystals to 550 °C (Supporting Information, Figure S12). MTCA-DMSO-30 yields a thick plate-like material still preserving the crystal morphology during polycondensation. For MTCA-DMSO/H_2O-30 and MTCA-H_2O-100 crystals, the inner part undergoes fast sublimation similar to MCA, resulting in the formation of hollow microtubes consisting of layered and flat sheets. The hollow structure is already formed at around 450 °C (Supporting Information, Figure S13). Thin 2D microsheets of g-CN aligned to the direction of π–π interaction were clearly observed in TEM image of MTCA-DMSO/H_2O-30-550 (Figure 3). The struc-

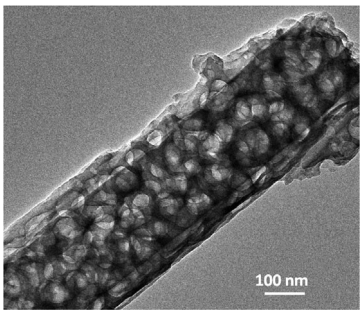

Figure 3. TEM image of MTCA-DMSO/H_2O-30-550.

tural shrinkage leads to the formation of macropores of 80–100 nm within the individual sheets. It can be expected that this porosity enhances the accessibility of catalytic sites inside the layered microsheets. The copolymerization of melamine with TCA yields an identical chemical and graphitic structure as observed for MCA-550 as is evidenced by FTIR and XRD analysis (Supporting Information, Figure S14, 15). Note that the pre-organized organic microcrystal (tens of micrometers in size) formed between melamine and TCA by the strong molecular interactions improves the chemical structure and probably the thermal stability of the resulting g-CN (Supporting Information, Figure S16). This is supported by the thermogravimetric analysis (TGA) in that about 30 wt % of the initial mass of MTCA-DMSO/H_2O-30 remains on heating to 300 °C, while less than 0.04 wt % for melamine and 20 wt % for TCA are left at the same temperature. Elemental analysis shows that the condensed material contains negligible amount of sulfur (< 0.8 wt %) above 450 °C, which is supported by XPS result showing no peaks at around 164 eV (Supporting Information, Figure S17).

UV/Vis diffuse reflectance spectra of MCA and MTCA crystals heated at 550 °C resemble the typical semiconductor absorption (Supporting Information, Figure S18). The absorption edges were slightly blue-shifted compared to that of Melamine-550, which is probably due to the formation of low-dimensional g-CN materials. Multiple reflections or transmission of light through the assembled structure remarkably enhance the optical absorption from 350 to 700 nm compared to Melamine-550.[18] The enhancement was less pronounced in MTCA-550 samples owing to large particle size, which can be simply modified by increasing the condensation temperature (Supporting Information, Figure S18 b,c). Further condensation of MTCA-DMSO/H_2O-30 above 600 °C yields a blue-shift of the absorption edge by

0.31 eV. This could be a hypsochromic shift that results from H-aggregates formation, as seen by a shift of the (002) peak to higher scattering angles in XRD analysis (Supporting Information, Figure S16). The optical bandgap values are listed in the Supporting Information, Table S1 with texture properties.

The efficient separation and migration of photoexcited carriers from the bulk to the surface catalytic sites was observed by time-resolved fluorescence spectroscopy and photocurrent measurement. We examined MTCA-DMSO/H_2O-30-600 with a large graphene area and a particle size that probably has higher charge recombination and electronic resistance than other g-CNs. Supporting Information, Figure S19 shows the decay spectra monitored at 520 nm. The lifetimes calculated by the triple-exponential decay model were increased at least twice compared to those of Melamine-550 (Supporting Information, Table S2). This shows significant suppression of charge recombination due to the formation of a highly condensed g-CN structure and the associated enhanced electronic conductivity. The photocurrent under visible light irradiation (>420 nm) was indeed greatly enhanced by 10 times compared to Melamine-550 (Supporting Information, Figure S20). It is also comparable to or even better than that of MCA-DMSO-30-550 possessing similar but smaller sheet-like structure. The 2D thin microsheets clearly facilitate the electronic transfer of charge carriers.

The photocatalytic activity of g-CNs synthesized from MCA and MTCA crystals was examined in the hydrogen evolution reaction from water using 3 wt% Pt as a co-catalyst and 10 vol% triethanolamine as an electron donor under visible light irradiation ($\lambda > 420$ nm). Melamine-550 has a hydrogen evolution rate (HER) of 30 μmol h^{-1}, corresponding to quantum efficiency (QE) of 0.26% (Figure 4a). MCA and MTCA samples showed a significant enhancement in HER by a factor of 4–9 (QE of ca. 2.3%) over Melamine-550. These samples heated at higher temperature usually exhibit higher HER due to the high surface area and enhanced light absorption. The HER of MCA and MTCA samples is stable or rather increases with time (Figure 4b), for which no deassembly of the nanostructure was observed after the reaction. The highly condensed structure provides g-CNs with better mechanical and chemical stability for the catalytic reactions. Indeed, no degradation of the catalytic activity was observed even after protonation in highly concentrated HCl (37 wt%). Rather, HER of the protonated sample showed further enhancement by 25% over the pristine sample. Figure 4c shows the wavelength dependence of the HER. The active wavelength of MCA and MTCA samples was as high as 600 nm. HER traces over the visible range of light match well with the UV/Vis spectra. This proves that the hydrogen evolution reaction was driven by the photoexcited electron/hole pairs generated in MCA and MTCA structures. No hydrogen was detected without the photocatalyst and light irradiation.

In summary, 3D macroscopic assemblies of low-dimensional g-CNs were successfully synthesized by simple organic cooperative synthesis. The structure of the hydrogen-bonded molecular assembly between triazine molecules (and thus the resulting g-CNs) was tailored to exhibit preferential growth by controlling the precipitation temperature, crystallization

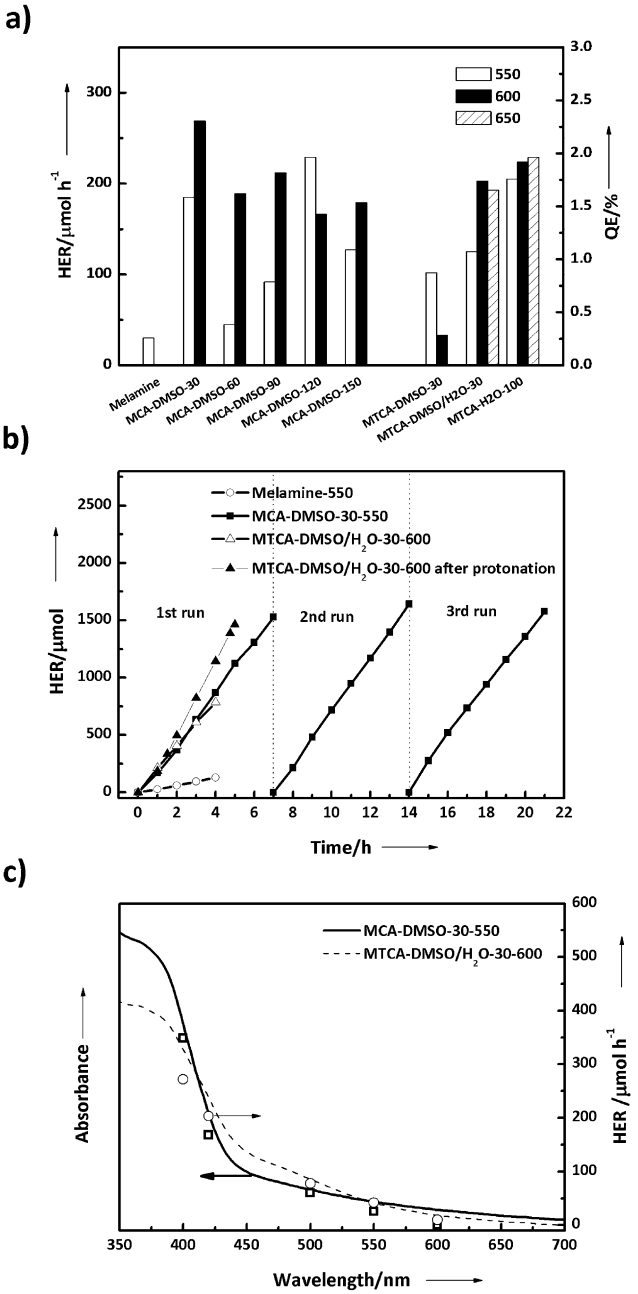

Figure 4. a) HER and corresponding QE of g-CNs synthesized from MCA and MTCA crystals. b) Stability test for 21 h. c) Wavelength dependence of HERs.

solvent, and hydrogen bonding donor–acceptor pair. The resulting self-supporting, 3D macroscopic material enabled us to characterize the cooperative properties and photocatalytic activities of low-dimensional g-CN materials. The present method should allow the design and synthesis of various g-CN-based structures and nanocomposites with specified dimension and chemical functionality. The above method may find strength in further functionalization by co-monomer control,[19] hybridization with graphene,[20] and device fabrication of g-CN.[21]

Received: May 10, 2013
Revised: August 3, 2013
Published online: September 13, 2013

Keywords: carbon nitrides · crystal engineering · hydrogen-bonded networks · photocatalysis · supramolecular chemistry

[1] a) P. Ball, L. Garwin, *Nature* **1992**, *355*, 761 – 766; b) A. N. Goldstein, C. M. Echer, A. P. Alivisatos, *Science* **1992**, *256*, 1425 – 1427.
[2] a) M. Bruchez, Jr., M. Moronne, P. Gin, S. Weiss, A. P. Alivisatos, *Science* **1998**, *281*, 2013 – 2016; b) T. S. Ahmadi, Z. L. Wang, T. C. Green, A. Henglein, M. A. El Sayed, *Science* **1996**, *272*, 1924 – 1926.
[3] a) Z. W. Pan, Z. R. Dai, Z. L. Wang, *Science* **2001**, *291*, 1947 – 1949; b) R. Tenne, L. Margulis, M. Genut, G. Hodes, *Nature* **1992**, *360*, 444 – 446; c) M. R. Ghadiri, J. R. Granja, R. A. Milligan, D. E. McRee, N. Khazanovich, *Nature* **1993**, *366*, 324 – 327.
[4] Z. P. Chen, W. C. Ren, L. B. Gao, B. L. Liu, S. F. Pei, H. M. Cheng, *Nat. Mater.* **2011**, *10*, 424 – 428.
[5] M. Li, H. Schnablegger, S. Mann, *Nature* **1999**, *402*, 393 – 395.
[6] Y. S. Zhao, H. B. Fu, F. Q. Hu, A. D. Peng, J. N. Yao, *Adv. Mater.* **2007**, *19*, 3554 – 3558.
[7] Y. S. Zhao, H. B. Fu, A. D. Peng, Y. Ma, D. B. Xiao, J. N. Yao, *Adv. Mater.* **2008**, *20*, 2859 – 2876.
[8] E. Kroke, M. Schwarz, *Coord. Chem. Rev.* **2004**, *248*, 493 – 532.
[9] A. Thomas, A. Fischer, F. Goettmann, M. Antonietti, J. O. Muller, R. Schlogl, J. M. Carlsson, *J. Mater. Chem.* **2008**, *18*, 4893 – 4908.
[10] Y. Wang, X. C. Wang, M. Antonietti, *Angew. Chem.* **2012**, *124*, 70 – 92; *Angew. Chem. Int. Ed.* **2012**, *51*, 68 – 89.
[11] a) M. Groenewolt, M. Antonietti, *Adv. Mater.* **2005**, *17*, 1789 – 1792; b) Y. J. Cui, Z. X. Ding, X. Z. Fu, X. C. Wang, *Angew. Chem.* **2012**, *124*, 11984 – 11988; *Angew. Chem. Int. Ed.* **2012**, *51*, 11814 – 11818; c) P. Niu, L. L. Zhang, G. Liu, H. M. Cheng, *Adv. Funct. Mater.* **2012**, *22*, 4763 – 4770; d) S. B. Yang, Y. J. Gong, J. S. Zhang, L. Zhan, L. L. Ma, Z. Y. Fang, R. Vajtai, X. C. Wang, P. M. Ajayan, *Adv. Mater.* **2013**, *25*, 2452 – 2456.
[12] a) Y.-S. Jun, E. Z. Lee, X. Wang, W. H. Hong, G. D. Stucky, A. Thomas, *Adv. Funct. Mater.* **2013**, *23*, 3661 – 3667; b) M. Shalom, S. Inal, C. Fettkenhauer, D. Neher, M. Antonietti, *J. Am. Chem. Soc.* **2013**, *135*, 7118 – 7121; c) K. Kailasam, J. D. Epping, A. Thomas, S. Losse, H. Junge, *Energy Environ. Sci.* **2011**, *4*, 4668 – 4674.
[13] A. Ranganathan, V. R. Pedireddi, G. Sanjayan, K. N. Ganesh, C. N. R. Rao, *J. Mol. Struct.* **2000**, *522*, 87 – 94.
[14] M. J. Bojdys, J. O. Muller, M. Antonietti, A. Thomas, *Chem. Eur. J.* **2008**, *14*, 8177 – 8182.
[15] X. J. Zhang, X. H. Zhang, W. S. Shi, X. M. Meng, C. S. Lee, S. T. Lee, *Angew. Chem.* **2007**, *119*, 1547 – 1550; *Angew. Chem. Int. Ed.* **2007**, *46*, 1525 – 1528.
[16] Y. S. Jun, W. H. Hong, M. Antonietti, A. Thomas, *Adv. Mater.* **2009**, *21*, 4270 – 4274.
[17] S. Ahn, J. Prakasha Reddy, B. M. Kariuki, S. Chatterjee, A. Ranganathan, V. R. Pedireddi, C. N. R. Rao, K. D. M. Harris, *Chem. Eur. J.* **2005**, *11*, 2433 – 2439.
[18] E. Z. Lee, Y. S. Jun, W. H. Hong, A. Thomas, M. M. Jin, *Angew. Chem.* **2010**, *122*, 9900 – 9904; *Angew. Chem. Int. Ed.* **2010**, *49*, 9706 – 9710.
[19] J. Zhang, G. Zhang, X. Chen, S. Lin, L. Moehlmann, G. Dolega, G. Lipner, M. Antonietti, S. Blechert, X. Wang, *Angew. Chem.* **2012**, *124*, 3237 – 3241; *Angew. Chem. Int. Ed.* **2012**, *51*, 3183 – 3187.
[20] A. J. Du, S. Sanvito, Z. Li, D. W. Wang, Y. Jiao, T. Liao, Q. Sun, Y. H. Ng, Z. H. Zhu, R. Amal, S. C. Smith, *J. Am. Chem. Soc.* **2012**, *134*, 4393 – 4397.
[21] a) F. Yang, M. Lublow, S. Orthmann, C. Merschjann, T. Tyborski, M. Rusu, S. Kubala, A. Thomas, R. Arrigo, M. Haevecker, T. Schedel-Niedrig, *ChemSusChem* **2012**, *5*, 1227 – 1232; b) K. Kailasam, J. Schmidt, H. Bildirir, G. Zhang, S. Blechert, X. Wang, A. Thomas, *Macromol. Rapid Commun.* **2013**, *34*, 1008 – 1013.

